Special Collection

Illumination Intensity Dependence of the Recombination Mechanism in Mixed Perovskite Solar Cells

Alejandra Castro-Chong[+],[a] Antonio J. Riquelme[+],[c] Tom Aernouts,[b] Laurence J. Bennett,[d] Giles Richardson,[d] Gerko Oskam,*[a, c] and Juan A. Anta*[c]

Recombination mechanisms in solar cells are frequently assessed through the determination of ideality factors. In this work we report an abrupt change of the value of the "apparent" ideality factor (n_{AP}) in high-efficiency $FA_{0.71}MA_{0.29}PbI_{2.9}Br_{0.1}$ based mesoscopic perovskite solar cells as a function of light intensity. This change is manifested as a transition from a regime characterized by $n_{AP}\sim1.8$–2.5 at low light intensities ($<10\ mWcm^{-2}$) to one characterized by $n_{AP}\sim1$. This transition is equally observed in the recombination resistance extracted from open-circuit impedance measurements. We use drift-diffusion simulations with explicit consideration of ion migration to determine the origin of this transition. We find that a change ofrecombination mechanism concurrent with a modification of the concentration of ionic vacancies is the most likely explanation of the observed behaviour. In the drift-diffusion simulations we show that the apparent ideality factor is in fact affected by the ion vacancy concentration so it is not the optimal parameter to assess the dominant recombination mechanism. We argue that a procedure based on a recently derived "electronic" ideality factor obtained from the high frequency feature of the impedance spectrum is better suited to determine the recombination route that dictates the photovoltage.

1. Introduction

The build-up and collection of charges in solar cells are determined by light absorption and carrier generation, and limited by charge carrier recombination, which determines the open-circuit voltage (V_{OC}). Recombination occurs through a combination of monomolecular (first-order), bimolecular (second-order), trap-assisted, and Auger recombination (third-order). Optimization of the power conversion efficiency relies on minimizing the recombination processes towards the radiative limit (Shockley-Queisser limit).[1] Therefore, identifying the carrier recombination mechanisms is fundamental for effectively designing photovoltaic devices.

The exact sources of nonradiative recombination in perovskite materials have not yet been identified. While the formation of defects is known to be highly probable in this type of material,[2] the carrier lifetime is still impressively long with τ of several hundreds of ns and even longer.[3,4] Yet, we have not seen Perovskite Solar Cells (PSCs) performing close to the radiative limit; thus, considerable scope remains for reducing nonradiative recombination in these devices. In general, in this type of solar cell, it has been claimed that the recombination processes that determine the V_{OC} are mainly governed by the defect physics of the perovskite layer bulk.[5–8] However, the importance of recombination at interfaces has been highlighted by several authors that showed that surface treatments greatly improve performance, presumably by suppressing recombination.[9,10]

The defect physics of the absorber plays a critical role in determining the nonradiative recombination behaviour. Perovskite materials exhibit unique defect properties, which is very much attributed to its well-established ion migration under illumination and electrical bias.[11,12] The ionic environment in PSCs can moderate the rate of charge injection and electron-hole recombination in a number of ways, such as electronic-ionic coupling, surface dipole introduction, and screening of the built-in electric field at the interfaces.[13–16] The interpretation of ionic-electronic coupling affecting the collection probability of photo-generated charges has gained strength. According to Pockett *et al.*, a new ionic distribution, upon light or electrical excitation, might be favourable in reducing the recombination rate through reduction in trap capture cross section and/or ionic modulation of the band offsets in the device.[13] Jacobs *et al.*, rationalized the manifestations of ion migration ("giant" photoinduced capacitance, inductive loop, and "negative" capacitance), as a phase delayed recombination current con-

[a] *Dr. A. Castro-Chong,[+] Prof. G. Oskam*
Department of Applied Physics, CINVESTAV-IPN
Antigua Carretera a Progreso km 6, Mérida, Yucatán 97310 (México)
E-mail: gosk@upo.es
[b] *Prof. T. Aernouts*
Thin-Film Photovoltaics – partner in EnergyVille and Solliance, imec
Thor Park 8320, 3600 Genk (Belgium)
[c] *A. J. Riquelme,[+] Prof. G. Oskam, Prof. J. A. Anta*
Department of Physical, Chemical and Natural Systems, Universidad Pablo de Olavide
Carretera de Utrera km 1, Sevilla 41013 (Spain)
E-mail: jaantmon@upo.es
[d] *L. J. Bennett, Prof. G. Richardson*
Mathematical Sciences, University of Southampton
Southampton SO17 1BJ (UK)
[+] *These authors contributed equally to this work.*

Supporting information for this article is available on the WWW under https://doi.org/10.1002/cplu.202100233

This article is part of a Special Collection on "Perovskite Materials and Devices"

tributing to the measured impedance at low frequencies.[16] Recently, some of us[17] confirmed this interpretation by comparing the characteristic response of the impedance of perovskite solar cells of different compositions[8,18] with the predictions of a drift-diffusion numerical model. The numerical simulations show that ionic redistribution at the transport layer interfaces gives rise to the low-frequency signal of the impedance spectrum and can produce negative capacitance features and loops in the complex plane. Although all these signals can be reproduced with trap-limited bulk-recombination only, the drift-diffusion simulations also show that surface recombination contributes significantly to the electrical losses in perovskite solar cells, and that this contribution is needed to fit both the experimental *J-V* curve and the impedance spectra.

The diode ideality factor is a key parameter, which is regularly adopted to analyse recombination losses occurring during solar cell operation.[19] Charge carrier kinetic properties at the interfaces and the generation of surface defects are among the features that have been identified by using ideality factors in PSCs.[6,7] In the classical theory, the diode ideality factor may be extracted from the analysis of the V_{OC} as a function of illumination intensity (*vide infra*).

However, Riquelme et al.[17] and Courtier[20] showed that, for PSCs, the measured values of the ideality factor depend not only on the type of recombination but also on the effect of ionic accumulation on the electric potential. Bearing this in mind, we define the *apparent ideality factor* n_{AP} via the diode equation:[6]

$$qV_{OC} = E_g - n_{AP}k_BT \ln\frac{I_0}{I}, \quad (1)$$

where E_g is the bandgap of the absorbing material, q is the elementary charge, k_B is the Boltzmann's constant, T is absolute temperature, and I is the light intensity (I_0 is a constant with the same units as I). Another method for determining n_{AP} is the Impedance Spectroscopy (IS) technique. The apparent diode ideality factor n_{AP} can also be calculated from the recombination resistance,[5,7,8]

$$R_{rec} = \left(\frac{\partial J_{rec}}{\partial V}\right)^{-1} = R_{00}exp\left[-\frac{qV_{OC}}{n_{AP}\,k_BT}\right] \quad (2)$$

where J_{rec} is the recombination current density and R_{00} is the resistance at zero potential.

When the classical theory is applied to perovskite solar cells, values of the apparent ideality factor varying from 1.4 to 2 have been associated with the Shockley-Read-Hall (SRH) recombination mechanism in the bulk,[5,21,22] with the lower values (<2) corresponding to solar cells based on mixed-cation lead mixed-halide perovskite materials.[7] Drift-diffusion simulations with explicit ionic motion by Riquelme et al.[17] confirm that the two routes used to obtain n_{AP}, (that is, either by using Eq. (1) or by using Eq. (2)), yield identical values of n_{AP} and predict $n_{AP}\sim 2$ when bulk SRH recombination is dominant and smaller values when surface recombination is significant. It is important to note that these numerical predictions were obtained for an ion vacancy concentration inferred from first-principles[2] and widely used in several numerical studies.[17,23,24]

Courtier[20] showed thatfor PSCsthe potential across the bulk of the perovskite layer is screened by charge accumulation at the interfaces, implying that the value of n_{AP} (termed in Ref.[20] as "ectypal factor") is approximately equal to the reciprocal of the proportion of the potential difference that forms a barrier to recombination. As a result, non-integer and voltage-dependent values are expected. In the case of bimolecular recombination, a value of 1 is predicted (as for the classical theory) because the whole potential difference forms a barrier to recombination. In the same way, surface recombination located at the metal/TL interfaces also gives rise to a value of 1. However, for bulk SRH, a value of around 2 is predicted only for a cell with an approximately symmetric potential distribution across the cell, while values above or below 2 may signify bulk SRH in an asymmetric cell. Surface recombination at the TL/perovskite interfaces can also return a range of values, depending on the distribution of the potential across the cell. All these results evidence how important it is to bear in mind that the ionic distribution (which determines the potential) impacts the measured value of n_{AP}.

In this study, the charge recombination mechanisms in $FA_{0.71}MA_{0.29}PbI_{2.9}Br_{0.1}$-based mesoscopic PSCs are investigated by means of the n_{AP} values extracted from the analysis of V_{OC} as a function of illumination intensity, Eq. (1), and from impedance spectroscopy (IS) measurements at open-circuit. Two different values of the n_{AP} were observed, depending on the illumination intensity. For low light intensity (<10 mW cm^{-2}), we found $n_{AP}=$ 2.4–1.8, pointing to recombination losses dominated by bulk SRH-type recombination in the perovskite layer. In contrast, for high light intensity (≥ 10 mW cm^{-2}) $n_{AP}=1.1$, which shows that a change in the governing recombination mechanism and/or in the ionic characteristics of the perovskite takes place when the concentration of photogenerated carriers exceeds a certain threshold. With the help of drift-diffusion simulations and novel theoretical insights[25] we discuss the origin of this change of regime.

2. Results

2.1. V_{OC} vs Illumination Intensity

Representative *J-V* curves at different illumination intensities are shown in Figure 1a. The recorded photovoltaic (PV) parameters of the devices illuminated at 1 sun ($I=100$ mW cm^{-2}) are: current density (J_{SC}) 23.5 ± 1.8 mA cm^{-2}, V_{OC} 1.1 ± 0.2 V, fill factor (*FF*) $67\pm2\%$ and conversion efficiency (*PCE*) $17.3\pm2.1\%$. The V_{OC} generated at 1 sun is close to 1.1 V, which is around or even above the values reported for similar perovskite compositions.[26,27] The open-circuit voltages (V_{OC}) generated at the different illumination intensities (0.5, 1, 3, 5, 10, 20, 40 and 100 mW cm^{-2}), are shown in Figure 1b. Two different slopes of the V_{OC} vs light intensity response were observed, depending on the illumination intensity. Following Eq. (1), the value of the n_{AP} was found to be 1.8, for low light intensity (<10 mW cm^{-2}),

while for high light intensity ($\geq 10\,mW\,cm^{-2}$) $n_{AP} = 1.1$. This crossover is an indication of a change in the recombination mechanism, but we cannot entirely rule out that this is an indicative of some other physical effect. A similar behaviour has been described by Caprioglio *et al.*[28,29] It is worth mentioning that here the V_{OC} values were only measured after the devices had reached steady state (50 to 200 s of initial delay). Furthermore, the devices were discharged before each new measurement by short-circuiting in the dark. The time required to reach a nearly null dark current was at least 60 s. With this protocol we intend to avoid uncertainty related to preconditioning and V_{OC} evolution due to slow ionic redistribution.

2.2. Impedance Spectroscopy

Representative Nyquist plots measured at open-circuit at the different irradiance values are shown in Figure 2. The impedance response is characterized by two semi-circles, one at high frequency (*hf*) from 10^3 to 10^5 Hz, and a second one at low frequency (*lf*) from 10^{-2} to 10^3 Hz. In Figure S1 *J-V* curves before and after the impedance experiment are reported, showing that there is no degradation of the cell during the small perturbation analysis. Bode plots corresponding to the Nyquist diagrams of Figure 2 are presented in Figure S2 in the Supporting Information.

The impedance spectra were fit using an equivalent circuit comprising a resistance R_s in series with two Voigt elements, Figure 2. Note that alternative equivalent circuits have also been employed successfully in the literature to fit the IS of perovskite solar cells. These are based on different physical interpretations. However, all of them generate two signals (arcs in the Nyquist plot) at low and high frequencies, respectively, and with almost identical fitting parameters for both their respective resistive and the capacitive components.[30–32] The equivalent circuit used here has the only purpose of providing a numerical frame to obtain the *hf* and *lf* resistances and the apparent ideality factor. For an interpretation of the impedance spectrum without equivalent circuits we refer the reader to references[33] and.[17]

The capacitive elements were modelled as a constant phase element *CPE*, with $Z_{CPE} = 1/Q(j\omega)^P$.[34] The *hf* arc has a shape that is close to a semicircle with *P* ranging from 0.9 to 1; while *P* is between 0.75 and 0.85, for the *lf* arc.

In Figure 3, the resistive (R_{lf} and R_{hf}) and capacitive (CPE_{lf} and CPE_{hf}) elements of the IS analysis are displayed as a function of the V_{OC} generated at the different irradiance values. In general, both R_{lf} and R_{hf} components decrease exponentially as the V_{OC} increases, as expected for a recombination resistance.[8,18,35] Contreras-Bernal *et al.*, reported that only the (apparent) ideality factor extracted from the slope of the logarithm of the R_{hf} strictly coincides with the (apparent) ideality factor derived from the slope of the V_{OC} vs illumination.[8] In addition, Riquelme *et al.*,[17] related the low frequency signal to charging/discharging of ionic accumulation layers at interfaces, which would produce a resistance and a CPE_{lf} with opposite slopes. Here, the apparent ideality factor n_{AP} was calculated using Eq. 2. We observe, for the first time, that both, R_{lf} and R_{hf} yield two different slopes depending on V_{OC}, consistent with the behaviour observed in the dependence of the V_{OC} with illumination intensity. Following Riquelme et al.[17] and Contreras-Bernal et al.[8] we extracted the ideality factor from the high frequency component. Specifically, $n_{AP} = 2.5$ for irradiance $I < 10\,mWcm^{-2}$ and $n_{AP} \sim 1$ for $I \geq 10\,mW\,cm^{-2}$ (Figure 3a, b). This behaviour was observed in three devices measured independently (Figure S3 in Supporting Information). In both regimes, the apparent ideality factor is approximately coincident with that obtained, in the conventional manner, from the V_{OC}-light intensity plot, confirming the internal consistency of Eqs. (1) and (2) and the reliability of the apparent ideality factors derived from the two types of experiment (steady state and small perturbation).

In this line of reasoning, it could be expected that using $R_{rec} = R_{lf} + R_{hf}$ in Eq. (2) would be a more sensible choice to extract the apparent ideality factor as this corresponds to the DC limit of the current-voltage response of the solar cell. However, using low frequency features of the spectra is more sensitive to non-reversible ionic migration and/or degradation of the device during the measurement. As shown theoretically in Ref.,[25] the slope of the R_{hf} -V_{oc} plot can be related to the apparent ideality factor, and explains the common experimental observation[5,8,17,22] that Eqs. (1) and (2) yield the same results when $R_{rec} = R_{hf}$.

The change of the apparent ideality factor with the illumination intensity is evidence that recombination takes place via a different mechanism, which depends on the concentration of charge carriers in the active layer. The low-irradiance n_{AP} values are the typical values reported for similar perovskite solar cells. This observation has been attributed to SRH (trap-mediated) recombination in the bulk.[5–7,22] However, at high irradiances, the n_{AP} values indicate a change in the dominant recombination mechanism, or, possibly, that some other physical change occurs within the cell.

The origins of the high and low-frequency capacitive components have been ascribed to different charge polarisation processes.[30,36–38] The CPE_{hf} is generally ascribed to the bulk dielectric response of the perovskite layer[32,35,39] and is defined as the geometric capacitance,

$$C = A\varepsilon/d. \tag{3}$$

where ε is the dielectric permittivity of the perovskite active layer, *A* is the surface area of the device, and *d* is the thickness of the perovskite. According to Eq. (3), the geometrical capacitance should be voltage independent. However, our results show that the CPE_{hf} increases exponentially with electric potential, although the slope is much smaller than that of the R_{hf}. The dependence with open circuit voltage could be (1) due to a chemical effect of charge accumulation in the mesoporous TiO_2 layer and/or in the perovskite[40,41] or (2) to a change in the permittivity, ε, of the perovskite material with illumination.[42,43] However, drift-diffusion simulations for a planar device (*vide infra*) also show exponential behaviour in this voltage interval. This suggests that accumulation of charges in the bulk of the

active layer could be the only mechanism needed to rationalize this experimental feature.

On the other hand, CPE_{lf} exhibits an exponential increase with V_{OC}, which is an ubiquitous observation in perovskite solar cells.[5,7,8,37,44,45] The low-frequency capacitance can be described by the following expression,[7]

$$C_{lf} = \frac{dQ}{dV} \propto exp\left[\frac{qV_{OC}}{\gamma\, k_B T}\right] \quad (4)$$

where Q is the charge per unit surface, and γ is an exponential coefficient that serves as a fitting parameter. This exponential dependence of the low frequency capacitance has been ascribed to charge accumulation at the interfaces.[42,44] However, it has been shown recently that charge accumulation alone, either ionic or electronic, is not sufficient to justify the very high values (of the order of 0.1–1 F/cm^2) of the capacitance observed in the impedance spectra of perovskite solar cells at low frequencies.[16] Thus, CPE_{lf} must contain two contributions: i) charge accumulation and ii) phase-delayed recombination current due to the ion displacement.[16,17]

Here, we observe that the CPE_{lf} displays two different slopes; exactly as the R_{lf}, with the same values but opposite sign, in accordance with the drift-diffusion simulations of Riquelme *et al.*[17] As this crossover takes places at the same values of voltage as the *high-frequency* resistance, which stems from recombination, we relate the *low-frequency* response to ionic-electronic coupling affecting the recombination current and thus the measured capacitance through a phase delayed response. This analysis is in line with the interpretation of Jacobs et al.[16] and Pockett et al.[46]

The time constant τ was calculated from the respective products RC, Figure 3d. As R_{lf} and CPE_{lf} have reciprocal slopes, the time constant was found to be nearly independent of light intensity in the low-frequency regime. This is what is normally observed in experiments[5,8,31,45–47] and predicted by drift-diffusion simulations.[17] In contrast, in the high-frequency regime the resistive and capacitive elements are uncoupled (they stem from different mechanisms, as explained above) and consequently the corresponding time constant displays a slight exponential dependence on illumination intensity.

In general, the steady-state and impedance results indicate the existence of two regimes occurring at different light intensities: i) at irradiance values $< 10\ mW\,cm^{-2}$ the apparent ideality factor is 1.8–2.5, and ii) at irradiance values $\geq 10\ mW\,cm^{-2}$ the apparent ideality factor is close to unity. Apparent ideality factors close to 2 have commonly been observed in perovskite solar cells with the TiO_2/PS/spiro architecture.[5,7,8,48] According to the classical theory, an ideality factor of 2 is usually considered an indication of trap-mediated (SRH type) recombination in the bulk of the active layer.[48] On the other hand, an ideality factor close to 1 can stem from two alternative recombination mechanisms: (1) band-to-band radiative recombination or (2) surface-recombination at the perovskite/transport layer interfaces (low selectivity of the contacts).[48] From the values of the open-circuit potentials at 1-sun illumination obtained for our devices, far from the radiative limit for mixed perovskites of ~1.3 V,[49] we can infer that (2) is the more likely explanation of the ideality factor measured at high irradiances. However, the reasons for surface recombination becoming more important at high irradiances is unclear. It is worth mentioning that Caprioglio *et al.*[28] also reported this abrupt change of the V_{oc} vs. light intensity slope and use this observation to draw a distinction between "internal" and "external" ideality factors. This indicates that a deeper understanding of the meaning of the (apparent) ideality factor, and the underlying mechanisms that govern recombination in perovskite solar cells, is much needed.

2.3. Drift-diffusion simulations

As stated previously, the ideality factor obtained from both the steady-state measurement of Figure 1b and the small-perturba-

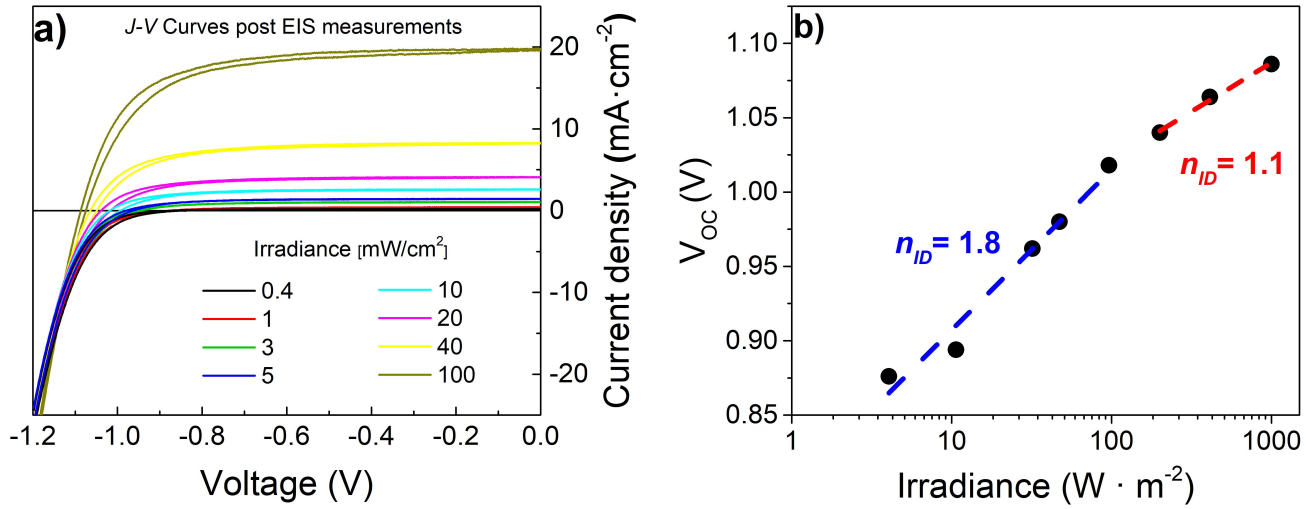

Figure 1. a) Representative current density-voltage curves of mesoscopic PSCs used for the IS analysis, under different irradiance values; the scan rate is 0.05 V s^{-1}. b) V_{OC} vs light intensity, lines show a logarithmic fit and the numbers indicate the n_{AP} obtained from the slope, according to Eq. 1.

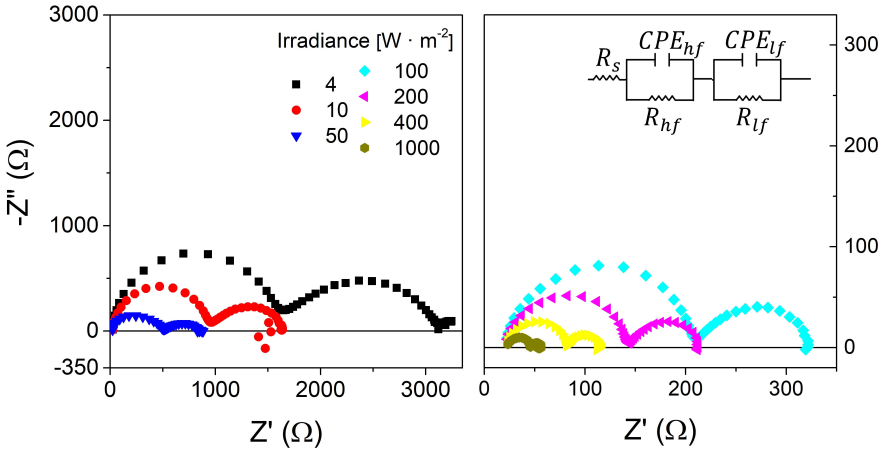

Figure 2. Nyquist plots measured at open circuit at the different irradiance values and equivalent electrical circuit used in the IS analysis. Left panel shows the spectra in the region where $n_{AP}\sim2$ (irradiance <10 mW cm^{-2}), and right panel the spectra where $n_{AP}\sim1$ (irradiance >10 mW cm^{-2}).

tion result of Figure 3a (obtained via Eqs. (1) and (2), respectively) is an "apparent" ideality factor that is not only determined by charge recombination mechanisms within the cell but also directly affected by the ionic distribution within the active layer. The effect of the ion vacancies in the perovskite layer are not considered by the classical diode theory used to infer the recombination mechanism from the apparent ideality factor. Indeed, Riquelme *et al.*[17] have used drift-diffusion simulations to show that the apparent ideality factor (obtained from steady-state and impedance measurements) changes in response to changes in the internal vacancy distribution. In this connection, an extension of the traditional diode equation, which takes account of ionic effects, has recently been proposed by Courtier,[50] and shows an ionic influence on n_{AP}, which should be considered when inferring the correct recombination mechanism.

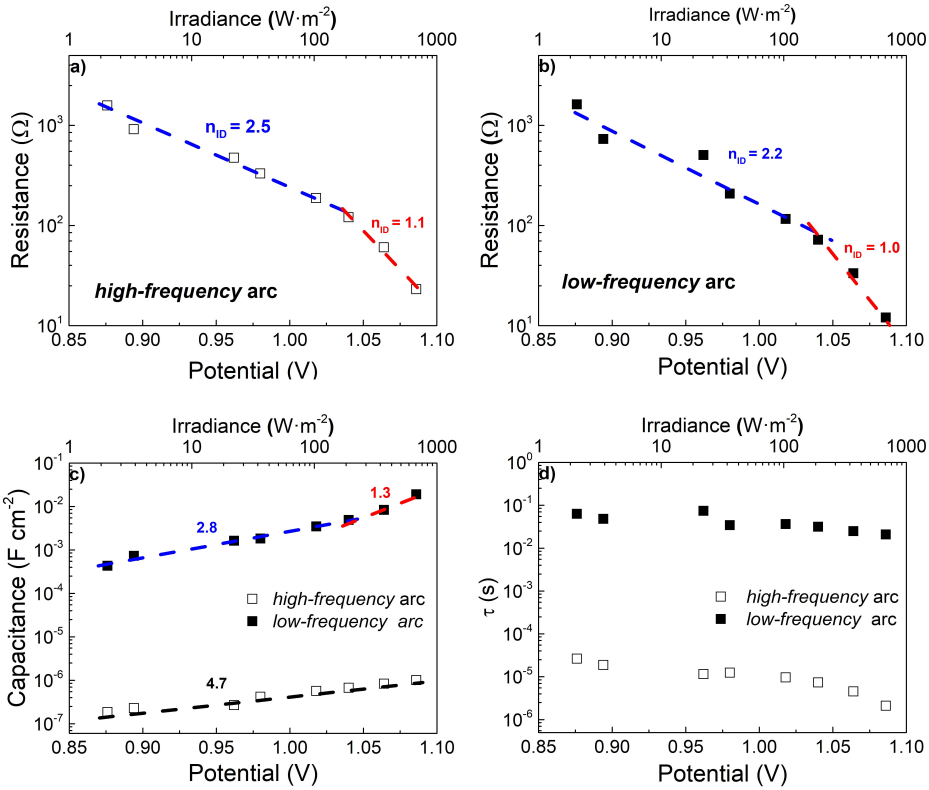

Figure 3. Electrical elements obtained from the IS analysis. a) and b) Resistive elements at the high and low frequency domains (R_{lf} and R_{hf}). c) and d) Capacitive elements (CPE_{lf} and CPE_{hf}) and time constant (τ). The lines correspond to the logarithmic fit and the numbers indicate the n_{AP} (N)/γ values extracted from the reciprocals of the slopes (Eqs. (2) and (4)).

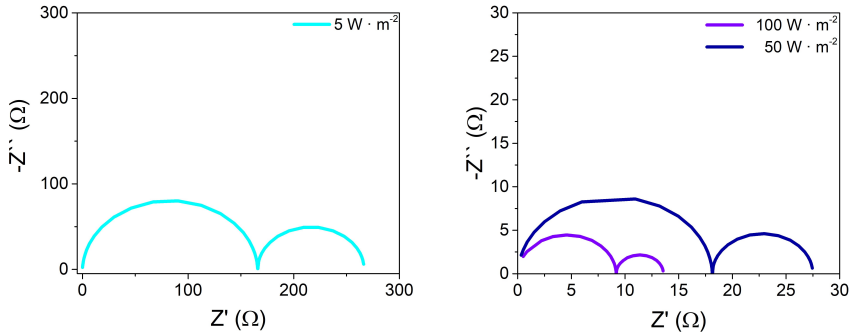

Figure 4. Simulated impedance spectra at open circuit at different light intensities for a mechanism where both bulk SRH recombination (electron lifetime[17] of 9 10^{-7} s) and surface recombination take place (recombination velocities at the TiO_2 and spiro interfaces, 20 and 10 m/s, respectively). The rest of the simulation parameters can be found in Table S1 in the Supporting Information.

To cast light on the origin of the change of slope in the steady state measurements and impedances with light intensity, we have run drift-diffusion simulations in which the relative weights of bulk and surface recombination, as well as the concentration of ionic vacancies are varied in order to see their impact on the spectra and the apparent ideality factor.

In Figure S4 in the Supporting Information we show simulation results when the bulk SRH mechanism is the only recombination route (apart from the always present bimolecular recombination). The drift-diffusion model predicts an apparent ideality factor of ~2 in this situation. However, the shape of the spectra is quite different to the experimental spectra recorded at low light intensities, with two arcs of comparable size (see Figure 2). In Figure 4 the effect of introducing surface recombination in addition to bulk recombination can be observed. The two arcs become of comparable size at all light intensities and the apparent ideality factor drops below 2, while still maintaining the consistency between steady-state and impedance values (Figure S5). In this case the simulated spectra have more resemblance to the measured spectra, and is similar to those previously reported in the literature for mixed perovskites.[47,51] As pointed out before, the model, which assumes a planar device with constant dielectric constant, predicts a slight exponential dependence of the high frequency capacitance at high voltages (Figure S6) in agreement with the experiment. This indicates that accumulation of charges at high voltages in the bulk of the active layer can be the cause of the increase of the high frequency capacitance. Hence, the model appears to provide a reasonably good description of the impedance response, indicating that both bulk SRH and surface recombination are required to best reflect experimental observations.

Hence, the change in the ideality factor can be explained as a transition towards a situation where recombination across the TiO_2 and spiro interfaces becomes progressively more important, as the cell is illuminated with a higher irradiance. Indeed, the modelling predicts a higher accumulation of electronic carriers and ions at the TiO_2 and spiro interfaces at high illumination intensities (see Figure S7 and S8 in the Supporting Information), in particular, more holes at the TiO_2 interface, and more electrons at the spiro one. This effect can promote enhanced surface recombination across the respective interfaces. Still, the simulated apparent ideality factor predicted for mixed bulk/surface recombination is well above the value of ~1 observed in the experiment at high light intensity (see Figure S5).

As mentioned previously, the apparent ideality factor n_{AP} as obtained from Eqs. (1) and (2) is actually affected by the ionic distribution. In Figure 5 we plot the apparent ideality factor predicted by the drift-diffusion model for two concentrations of ion vacancies in the active layer, one characteristic of MAPI perovskite as used in Refs.[17,24] and another reduced by a factor of ten. Two important conclusions can be extracted from this figure: (1) The value of n_{AP} decreases as we increase the surface recombination velocities and (2) the value of n_{AP} is lower, for lower concentrations of ionic vacancies. The simulation results points to a mixed mechanism to explain the experimental behaviour: an increase of surface recombination[29] and a diminution of ionic vacancies as we move from low to high illumination intensities. Additionally, in Figure 5 we plot the value of the "electronic ideality factor" (determined using eq.(7), *vide infra*).

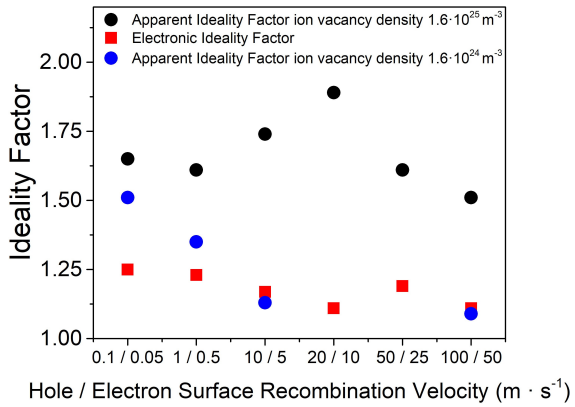

Figure 5. Apparent ideality factor and electronic ideality factor as predicted by the drift-diffusion model as a function of the surface recombination velocities (holes at the ETL interface and electrons at the HTL interface) and two values of the ion vacancy density. Note that the electronic ideality factor is the same (within the numerical error) for both values of the vacancy density.

It is a real possibility that the number of ionic vacancies can vary with illumination in organic lead halide perovskites. Mosconi et al. described a mechanism of vacancy-ion annihilation in the $MAPbI_3$ perovskite.[52] Several authors have also reported "defect curing" effects upon illumination,[53] also for mixed perovskites.[54] There are also studies in the literature where a beneficial effect of light soaking is reported, via a reduction of structural defects and/or ionic migration.[55,56] However, it is important to note that there are also reports where increases of photoconductivity upon illumination for isolated perovskite films are observed,[57] attributed to formation of defects and subsequent generation of iodine. Weber et al. described a mechanism of ionic defect formation upon application of light or electric fields.[58] This formation of ionic defects upon illumination also has a theoretical interpretation.[59] In spite of these divergent works, Motti and coworkers[60] showed theoretically that processes of "defect curing" and "defect formation" can actually coexist and compete. This means that a plethora of behaviours can be found depending on the nature and the preparation routes of the perovskite. In this case, in view of the drift-diffusion simulation results, a reduction of the number of mobile ions, at high irradiance, can offer the best plausible explanation for the simultaneous reduction of the apparent ideality factor observed in both the steady-state V_{oc} measurements and the impedance. The concurrent enhancement of surface recombination can also contribute to this change of regime when the illumination intensity is high enough.

The influence of the concentration of ionic vacancies on the apparent ideality factor shows the necessity of an alternative definition of the ideality factor that is independent of the density and distribution of ionic vacancies and which therefore only reflects purely electronic effects. Very recently Bennett and coworkers[25] have devised an analytic theory where the recombination current induced by a small electric perturbation near open circuit is

$$J_{rec}(V) = J_0 exp\left[\frac{qF(Q)}{k_b T} - \frac{qdE(t)}{n_{el} k_b T}\right] \quad (5)$$

where $F(Q)$ is a function that depends on the ionic distribution only, $E(t)$ is the transient electric field acting within the perovskite layer in the impedance experiment and n_{el} is the so-called electronic ideality factor. Eq. (5) is the generalization of the result reported by Courtier (Eq. (5) in Ref.[50]) under the assumption that the transient electric field is very small in comparison with the steady-state electrical bias V. This is one of the main requirements on which impedance spectroscopy, as a *small-perturbation technique*, is based.

Due to the slow migration of the ions, the steady-state ionic distribution is not perturbed during high frequency impedance measurements. Therefore, at high frequencies, $F(Q)$ is voltage-independent. Since the electric field induced by the applied voltage perturbation is given by $E = -V/d$, and knowing that the resistance is the reciprocal of the voltage derivative of the current, taking the voltage derivative of Eq. (5), we find that the electronic ideality factor can be obtained from

$$n_{el} = \frac{qR_{hf}\, J_{rec}(V_{DC})}{k_b T} \quad (6)$$

Obtaining the electronic ideality factor from *hf*impedance measurements is explained further in Ref.[25] In this work it is shown that the electronic ideality factor is a true analogue of the classical ideality factor, that is valid for the coupled electronic-ionic physics of perovskite solar cells. As such, it can be used to appropriately determine the dominant recombination mechanism, in the same way the ideality factor is used in classical theory.

In Figures 5 and 6 the electronic ideality factor obtained via Eq. (6) from the simulations and the experiments is compared with the apparent ideality factor obtained from Eqs. (1) and (2). As expected, n_{el} is found to be the same for different concentration of ionic vacancies (only n_{AP} is changed by modifying the concentration of vacancies). This result is confirmed in the simulations of Figure 5. On the other hand, n_{el} becomes smaller as the contribution of surface recombination is increased, reflecting the change of recombination mechanism. This behaviour is also observed in the experimental data of Figure 6, where this parameter moves from values larger than 2 ± 0.25 at low light intensity to values close to unity at high intensity. The apparent ideality factor n_{AP} reaches higher values, but also shows a tendency to lower its value as the light intensity is increased. As mentioned previously, this parameter depends on the ionic density, which appears to decrease when the cell is subjected to higher irradiance. As shown by the simulation, in Figure 6, only when the ion density is sufficiently low, the apparent ideality factor attains a value as low as 1. In summary, the transition observed in the experiments appears to be a combination of a change of recombination mechanism (with a growing contribution coming from surface recombination) and a reduction of the density of ionic defects in the perovskite material as the light intensity is increased.

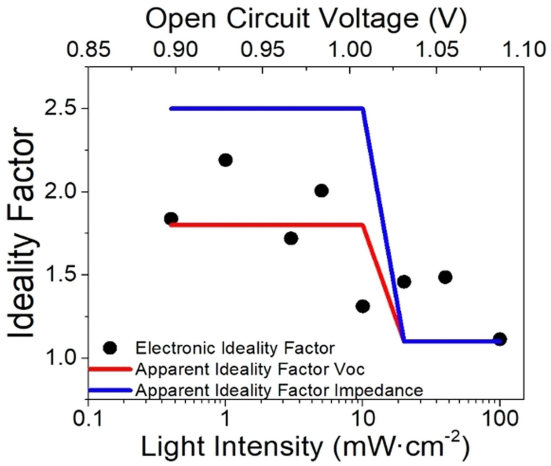

Figure 6. Apparent ideality factor (n_{AP}) and electronic ideality factor (n_{el}) as derived from Eqs. (1), (2) and (6) with the experimental results of Figure 2.

3. Conclusions

We have observed a change of behaviour of the recombination-related parameters in mesoscopic mixed perovskite ($FA_{0.71}MA_{0.29}PbI_{2.9}Br_{0.1}$) solar cells with changes in illumination intensity. This feature appears to be a crossover from a regime characterized by an apparent ideality factor of 1.8–2.5 at low irradiances, to another characterized by an ideality factor approaching unity, at high irradiances. This change of regime is observed in steady-state measurements of the open-circuit potential, and in small-perturbation impedance measurements at open circuit, both as a function of the light intensity. The transition takes place in both experiments at potentials of 1.03 V corresponding to an AM1.5G irradiance of 10 mW cm^{-2}. With the help of drift-diffusion simulations we attribute this peculiar behaviour to a combination of two effects. The first of these effects corresponds to a transition from a regime in which surface recombination across the transport layer interfaces is less important than bulk SRH recombination in the perovskite, to another one where surface recombination is dominant. The second of these effects corresponds to a reduction of ionic vacancies in the perovskite active layer with increases in illumination intensity, leading to a reduction of the values of the apparent ideality factor. Drift-diffusion simulations show that the apparent ideality factor derived from steady-state measurements of the open-circuit potential versus light intensity or, equivalently, from the high frequency resistance extracted from the impedance spectra is actually affected by the concentration of mobile ionic vacancies present in the perovskite material. A description based on the "electronic" ideality factor, extractable from the high frequency feature of the impedance spectrum, turns out to be a better tool with which to determine the dominant recombination mechanism in a particular solar cell configuration.

Experimental Section

Device Fabrication

Mesoscopic TiO_2-based PSCs were prepared using the mixed perovskite $FA_{0.71}MA_{0.29}PbI_{2.9}Br_{0.1}$. Glass substrates patterned with ITO were cleaned in an ultrasonic bath sequentially immersed in detergent, deionized water, acetone and iso-propanol. Subsequently, a 20-nm thick compact TiOx layer was deposited through e-beam evaporation (Angstrom Engineering) of Ti at a rate of 1 Å/s using a partial O_2 pressure of 1.7×10^{-4} Torr. Consecutively, a 120-nm mesoporous TiO_2 layer was prepared by spin-coating an anatase dispersion in ethanol at 1.2 wt%: 60 μL were spin-coated at 4500 rpm for 30 s; the number of repetitions was adjusted to achieve the desired thickness. The films were annealed at 450 °C for 30 min. The mixed perovskite absorbing material was prepared through the intramolecular exchange method as reported by Seok *et al.*,[61] using the two-step spin coating sequential process.[27,62] Using this methodology, two solutions are prepared: solution A consists of 1.25 M PbI_2 in a mixture of N, N-dimethyl formamide and dimethyl sulfoxide (DMF/DMSO: 90/10, v/v) and solution B consists of $CH(NH_2)_2I$ (FAI), CH_3NH_3I (MAI) and CH_3NH_3Br (MABr) (71:19:10 molar ratio) in isopropanol. The solution chemistry and spin coating conditions were selected for proper infiltration of a 120-nm-thick mesoporous TiO_2 layer, according to Castro-Chong *et al.*[51] Spiro-OMeTAD ("spiro") and Au were used as hole transport layer and electrode, respectively; following our previous report.[51]

Characterization

The photovoltaic characteristics of the devices were measured under ambient atmosphere using an Autolab PGSTAT302 N and a xenon arc lamp, Oriel 66924 equipped with AM 1.5G and water filters; calibration was performed with a Newport calibrated reference Si solar cell with an incorporated KG-5 optical filter. The devices were measured from forward to reverse bias and from reverse to forward bias, at a scan rate of 0.05 V s^{-1}, using a shadow mask to define the pixel active area of 0.08 cm^2.

IS was performed on the mesoscopic PSCs with PCE ~17%. The impedance response of the three devices, with 12 individual pixels each, was investigated at open-circuit potential (V_{OC}) using a Gamry electrochemical workstation. The V_{OC} was set by controlling the light intensity of a Xe-arc lamp with an AM 1.5G optical filter and a 10 cm water filter. Impedance measurements were performed at eight different illumination intensities: 0.4, 1, 3, 5, 10, 20, 40 and 100 mW cm^{-2}. The spectra were recorded from 10^6 Hz to 10^{-2} Hz, using an amplitude of 10 mV(rms). To minimize the effect of degradation of the devices in the analysed results, the spectra were recorded starting from the lower illumination intensity working up to the highest; the V_{OC} and *J-V* curve were monitored throughout the recorded spectra (Figure S1), to ensure the reliability of the data. A similar protocol has been suggested by Pitarch-Tena *et al.*[63]

Drift-diffusion modelling

Impedance spectra are numerically simulated using the *IonMonger* code,[64,65] which considers a fully-coupled one-dimensional drift-diffusion model that accounts for the motion of electrons, holes and positive anion vacancies within a planar perovskite solar cell. The cell is modelled as a three-layer structure in which a perovskite absorber layer is sandwiched between doped electron and hole transport layers. Further details of the model can be found in the works of Richardson *et al*[23] and Courtier *et al*,[24] where it was first developed, and a complete description of the modelling assumptions and model equations are given in the Supporting Information. The key model parameters are listed in Table S1 in the Supporting Information.

Impedance spectra are simulated by applying a sinusoidal voltage perturbation of the form

$$V_{ap}(t) = V_{DC} + V_p \boldsymbol{sin}(\omega t) \tag{7}$$

where V_{DC} is the DC voltage, V_p is the amplitude and ω is the angular frequency of the perturbation. In the simulations, the cell is perturbed about a steady state so that the phase and amplitude of the current response is stable in time. For each frequency, the current response is analysed using a Fourier transform to extract its phase and amplitude. This enables the impedance to be calculated and a spectrum to be constructed by obtaining solutions to the model for 40–100 frequencies over a wide frequency range.

Acknowledgements

This work was funded by the Ministerio de Ciencia e Innovación of Spain, Agencia Estatal de Investigación (AEI) and EU (FEDER)

under grants PID2019-110430GB-C22 and PCI2019-111839-2 (SCALEUP) and Junta de Andalucia under grant SOLARFORCE (UPO-1259175). The work was also funded by AMEXCID SRE-Conacyt-2016-1-278320, and the Royal Society under grant number ICA-R1-191321. The authors gratefully acknowledge support from the Ministerio de Universidades and Universidad Pablo de Olavide through the Beatriz Galindo program under project BEAGAL 18/00077 and grant BGP 18/00060. AJR thanks the Spanish Ministerio de Educación, Cultura y Deporte for its supports via a PhD grant (FPU2017-03684). LJB is supported by an EPSRC funded studentship from the CDT in New and Sustainable Photovoltaics, reference EP/L01551X/1. Funding for open access publishing: Universidad Pablo de Olavide/CBUA We thank Dr. Courtier for her extremely useful comments and discussions about this work.

Conflict of Interest

The authors declare no conflict of interest.

Keywords: diode ideality factor · impedance spectroscopy · ionic-electronic coupling mixed perovskite solar cells · recombination mechanisms

[1] W. Shockley, H. Queisser, *J. Appl. Phys.* **1961**, *32*, 510.
[2] C. Eames, J. M. Frost, P. R. F. Barnes, B. C. O'Regan, A. Walsh, M. S. Islam, *Nat. Commun.* **2015**, *6*, 7497.
[3] S. D. Stranks, G. E. Eperon, G. Grancini, C. Menelaou, M. J. P. Alcocer, T. Leijtens, L. M. Herz, A. Petrozza, H. J. Snaith, *Science* **2013**, *342*, 341–344.
[4] D. Kiermasch, P. Rieder, K. Tvingstedt, A. Baumann, V. Dyakonov, *Sci. Rep.* **2016**, *6*, 1–7.
[5] L. Contreras-Bernal, M. Salado, A. Todinova, L. Calio, S. Ahmad, J. Idígoras, J. A. Anta, *J. Phys. Chem. C* **2017**, *121*, 9705–9713.
[6] W. Tress, M. Yavari, K. Domanski, P. Yadav, B. Niesen, J. P. C. Baena, A. Hagfeldt, M. Graetzel, *Energy Environ. Sci.* **2018**, *11*, 151–165.
[7] O. Almora, K. T. Cho, S. Aghazada, I. Zimmermann, G. J. Matt, C. J. Brabec, M. K. Nazeeruddin, G. Garcia-Belmonte, *Nano Energy* **2018**, *48*, 63–72.
[8] L. Contreras-Bernal, S. Ramos-Terrón, A. Riquelme, P. P. Boix, J. Idígoras, I. Mora-Seró, J. A. Anta, *J. Mater. Chem. A* **2019**, *7*, 12191–12200.
[9] M. Stolterfoht, C. M. Wolff, J. A. Márquez, S. Zhang, C. J. Hages, D. Rothhardt, S. Albrecht, P. L. Burn, P. Meredith, T. Unold, D. Neher, *Nat. Energy* **2018**, *3*, 847.
[10] M. Stolterfoht, P. Caprioglio, C. M. Wolff, J. A. Márquez, J. Nordmann, S. Zhang, D. Rothhardt, U. Hörmann, Y. Amir, A. Redinger, L. Kegelmann, F. Zu, S. Albrecht, N. Koch, T. Kirchartz, M. Saliba, T. Unold, D. Neher, *Energy Environ. Sci.* **2019**, *12*, 2778–2788.
[11] W.-J. Yin, T. Shi, Y. Yan, *Cit. Appl Phys Lett* **2014**, *104*, 63903.
[12] J. M. Azpiroz, E. Mosconi, J. Bisquert, F. De Angelis, *Energy Environ. Sci.* **2015**, *8*, 2118–2127.
[13] A. Pockett, G. E. Eperon, N. Sakai, H. J. Snaith, L. M. Peter, P. J. Cameron, *Phys. Chem. Chem. Phys.* **2017**, *19*, 5959–5970.
[14] A. Guerrero, J. You, C. Aranda, Y. S. Kang, G. Garcia-Belmonte, H. Zhou, J. Bisquert, Y. Yang, *ACS Nano* **2016**, *10*, 218–224.
[15] R. A. Belisle, W. H. Nguyen, A. R. Bowring, P. Calado, X. Li, S. J. C. Irvine, M. D. McGehee, P. R. F. Barnes, B. C. O'Regan, *Energy Environ. Sci.* **2017**, *10*, 192–204.
[16] D. A. Jacobs, H. Shen, F. Pfeffer, J. Peng, T. P. White, F. J. Beck, K. R. Catchpole, *J. Appl. Phys.* **2018**, *124*, DOI 10.1063/1.5063259.
[17] A. Riquelme, L. J. Bennett, N. E. Courtier, M. J. Wolf, L. Contreras-Bernal, A. B. Walker, G. Richardson, J. A. Anta, *Nanoscale* **2020**, *12*, 17385–17398.
[18] I. Zarazúa, S. Sidhik, T. Lopéz-Luke, D. Esparza, E. De La Rosa, J. Reyes-Gomez, I. Mora-Seró, G. Garcia-Belmonte, *J. Phys. Chem. Lett.* **2017**, *8*, 6073–6079.
[19] J. Nelson, *The Physics of Solar Cells*, Imperial College Press, World Scientific Publishing Co., **2003**.
[20] N. E. Courtier, *Phys. Rev. Appl.* **2020**, *14*, 024031.
[21] A. Gagliardi, A. Abate, *ACS Energy Lett.* **2018**, *3*, 163–169.
[22] I. Zarazua, G. Han, P. P. Boix, S. Mhaisalkar, F. Fabregat-Santiago, I. Mora-Seró, J. Bisquert, G. Garcia-Belmonte, *J. Phys. Chem. Lett.* **2016**, *7*, 5105–5113.
[23] G. Richardson, S. E. J. O'Kane, R. G. Niemann, T. A. Peltola, J. M. Foster, P. J. Cameron, A. B. Walker, *Energy Environ. Sci.* **2016**, *9*, 1476–1485.
[24] N. E. Courtier, J. M. Cave, J. M. Foster, A. B. Walker, G. Richardson, *Energy Environ. Sci.* **2018**, *12*, 396–409.
[25] L. J. Bennett, A. J. Riquelme, N. E. Courtier, J. A. Anta, G. Richardson, *ArXiv210511226 Cond-Mat Physicsphysics* **2021**.
[26] T. Jesper Jacobsson, J.-P. Correa-Baena, M. Pazoki, M. Saliba, K. Schenk, M. Grätzel, A. Hagfeldt, *Energy Environ. Sci.* **2016**, *9*, 1706–1724.
[27] W. Qiu, J. P. Bastos, S. Dasgupta, T. Merckx, I. Cardinaletti, M. V. C. Jenart, C. B. Nielsen, R. Gehlhaar, J. Poortmans, P. Heremans, I. McCulloch, D. Cheyns, *J. Mater. Chem. A* **2017**, *5*, 2466–2472.
[28] P. Caprioglio, M. Stolterfoht, C. M. Wolff, T. Unold, B. Rech, S. Albrecht, D. Neher, *Adv. Energy Mater.* **2019**, *9*, 1901631.
[29] P. Caprioglio, C. M. Wolff, O. J. Sandberg, A. Armin, B. Rech, S. Albrecht, D. Neher, M. Stolterfoht, *Adv. Energy Mater.* **2020**, *10*, 2000502.
[30] A. Guerrero, G. Garcia-Belmonte, I. Mora-Sero, J. Bisquert, Y. S. Kang, T. J. Jacobsson, J.-P. Correa-Baena, A. Hagfeldt, *J. Phys. Chem. C* **2016**, *120*, 8023–8032.
[31] S.-M. Yoo, S. J. Yoon, J. A. Anta, H. J. Lee, P. P. Boix, I. Mora-Seró, *Joule* **2019**, *3*, 2535–2549.
[32] A. Todinova, L. Contreras-Bernal, M. Salado, S. Ahmad, N. Morillo, J. Idígoras, J. A. Anta, *ChemElectroChem* **2017**, *4*, 2891–2901.
[33] D. A. Jacobs, H. Shen, F. Pfeffer, J. Peng, T. P. White, F. J. Beck, K. R. Catchpole, *J. Appl. Phys.* **2018**, *124*, 225702.
[34] G. J. Brug, A. L. G. van den Eeden, M. Sluyters-Rehbach, J. H. Sluyters, *J. Electroanal. Chem. Interfacial Electrochem.* **1984**, *176*, 275–295.
[35] A. Pockett, G. E. Eperon, T. Peltola, H. J. Snaith, A. Walker, L. M. Peter, P. J. Cameron, *J. Phys. Chem. C* **2015**, *7*, 3456–3465.
[36] E. J. Juarez-Perez, R. S. Sanchez, L. Badia, G. Garcia-Belmonte, Y. S. Kang, I. Mora-Sero, J. Bisquert, *J. Phys. Chem. Lett.* **2014**, *5*, 2390–2394.
[37] O. Almora, I. Zarazua, E. Mas-Marza, I. Mora-Sero, J. Bisquert, G. Garcia-Belmonte, *J. Phys. Chem. Lett.* **2015**, *6*, 1645–1652.
[38] L. Contreras, J. Idígoras, A. Todinova, M. Salado, S. Kazim, S. Ahmad, J. A. Anta, *Phys. Chem. Chem. Phys.* **2016**, *18*, 31033–31042.
[39] J.-P. Correa-Baena, S.-H. Turren-Cruz, W. Tress, A. Hagfeldt, C. Aranda, L. Shooshtari, J. Bisquert, A. Guerrero, *ACS Energy Lett.* **2017**, *2*, 681–688.
[40] S. Wheeler, D. Bryant, J. Troughton, T. Kirchartz, T. Watson, J. Nelson, J. R. Durrant, *J. Phys. Chem. C* **2017**, *121*, 13496–13506.
[41] J. Jiménez-López, B. M. D. Puscher, D. M. Guldi, E. Palomares, *J. Am. Chem. Soc.* **2020**, *142*, 1236–1246.
[42] O. Almora, C. Aranda, G. Garcia-Belmonte, *J. Phys. Chem. C* **2018**, *122*, 13450–13454.
[43] M. J. Hong, L. Zhu, C. Chen, L. Tang, Y. H. Lin, W. Li, R. Johnson, S. Chattopadhyay, H. J. Snaith, C. Fang, J. G. Labram, *J. Am. Chem. Soc.* **2020**, *142*, 19799–19803.
[44] I. Zarazúa, J. Bisquert, G. Garcia-Belmonte, *J. Phys. Chem. Lett.* **2016**, 7, 525–528.
[45] I. Zarazúa, S. Sidhik, T. Lopéz-Luke, D. Esparza, E. De la Rosa, J. Reyes-Gomez, I. Mora-Seró, G. Garcia-Belmonte, *J. Phys. Chem. Lett.* **2017**, 8, 6073–6079.
[46] A. Pockett, G. E. Eperon, N. Sakai, H. J. Snaith, L. M. Peter, P. J. Cameron, *Phys. Chem. Chem. Phys.* **2017**, *19*, 5959–5970.
[47] O. Almora, K. T. Cho, S. Aghazada, I. Zimmermann, G. J. Matt, C. J. Brabec, M. K. Nazeeruddin, G. Garcia-Belmonte, *Nano Energy* **2018**, *48*, 63–72.
[48] W. Tress, M. Yavari, K. Domanski, P. Yadav, B. Niesen, J. P. C. Baena, A. Hagfeldt, M. Graetzel, *Energy Environ. Sci.* **2018**, *11*, 151–165.
[49] W. Tress, *Adv. Energy Mater.* **2017**, *7*, 1602358.
[50] N. E. Courtier, "Interpreting ideality factors for planar perovskite solar cells: Ectypal diode theory for steady-state operation," can be found under https://journals.aps.org/prapplied/accepted/ee07fA8bDed1b-d0412a70ae4369effc5fb0f6d794, n.d.
[51] A. Castro-Chong, W. Qiu, J. Bastos, N. Tchamba Yimga, R. García-Rodríguez, J. Idígoras, J. A. Anta, T. Aernouts, G. Oskam, *Sol. Energy* **2020**, *201*, 836–845.
[52] E. Mosconi, D. Meggiolaro, H. J. Snaith, S. D. Stranks, F. D. Angelis, *Energy Environ. Sci.* **2016**, *9*, 3180–3187.

[53] D. W. deQuilettes, W. Zhang, V. M. Burlakov, D. J. Graham, T. Leijtens, A. Osherov, V. Bulović, H. J. Snaith, D. S. Ginger, S. D. Stranks, *Nat. Commun.* **2016**, *7*, 11683.
[54] F. Zheng, X. Wen, T. Bu, S. Chen, J. Yang, W. Chen, F. Huang, Y. Cheng, B. Jia, *ACS Appl. Mater. Interfaces* **2018**, *10*, 31452–31461.
[55] H.-S. Kim, A. Hagfeldt, *Adv. Opt. Mater.* **2019**, *7*, 1801512.
[56] A. Pockett, D. Raptis, S. M. P. Meroni, J. Baker, T. Watson, M. Carnie, *J. Phys. Chem. C* **2019**, *123*, 11414–11421.
[57] G. Y. Kim, A. Senocrate, T.-Y. Yang, G. Gregori, M. Grätzel, J. Maier, *Nat. Mater.* **2018**, *17*, 445–449.
[58] S. A. L. Weber, I. M. Hermes, S.-H. Turren-Cruz, C. Gort, V. W. Bergmann, L. Gilson, A. Hagfeldt, M. Graetzel, W. Tress, R. Berger, *Energy Environ. Sci.* **2018**, *11*, 2404–2413.
[59] D. Barboni, R. A. D. Souza, *Energy Environ. Sci.* **2018**, DOI 10.1039/C8EE01697F.
[60] S. G. Motti, D. Meggiolaro, A. J. Barker, E. Mosconi, C. A. R. Perini, J. M. Ball, M. Gandini, M. Kim, F. De Angelis, A. Petrozza, *Nat. Photonics* **2019**, *13*, 532–539.
[61] W. S. Yang, J. H. Noh, N. J. Jeon, Y. C. Kim, S. Ryu, J. Seo, S. Il Seok, *Science* **2015**, *348*, 1234–7.
[62] M. L. Davies, M. Carnie, P. J. Holliman, A. Connell, P. Douglas, T. Watson, C. Charbonneau, J. Troughton, D. Worsley, *Energ. Mater. Mater. Sci. Eng. Energ. Syst.* **2014**, *9*, 482–485.
[63] D. Pitarch-Tena, T. T. Ngo, M. Vallés-Pelarda, T. Pauporté, I. Mora-Seró, *Impedance Spectroscopy Measurements in Perovskite Solar Cells: Device Stability and Noise Reduction*, American Chemical Society, **2018**.
[64] N. E. Courtier, J. M. Cave, A. B. Walker, G. Richardson, J. M. Foster, *J. Comput. Electron.* **2019**, *12*, 396–409.
[65] N. E. Courtier, G. Richardson, J. M. Foster, *Appl. Math. Model.* **2018**, *63*, 329–348.

Manuscript received: May 25, 2021
Revised manuscript received: August 30, 2021
Accepted manuscript online: August 31, 2021